Journal of Catalysis 261 (2009) 60–65

Contents lists available at ScienceDirect

Journal of Catalysis

www.elsevier.com/locate/jcat

Bromine-promoted PtZn is very effective for the chemoselective hydrogenation of crotonaldehyde

Ewan Galloway [a], Marc Armbrüster [a], Kirill Kovnir [b], Mintcho S. Tikhov [a], Richard M. Lambert [a,*]

[a] Department of Chemistry, University of Cambridge, Lensfield Road, Cambridge, CB2 1EW, UK
[b] Max-Planck-Institut für Chemische Physik fester Stoffe, Nöthnitzer Str. 40, 01187 Dresden, Germany

ARTICLE INFO

Article history:
Received 18 September 2008
Revised 31 October 2008
Accepted 4 November 2008
Available online 29 November 2008

Keywords:
PtZn
Intermetallic compound
Heterogeneous catalysis
Chemoselective hydrogenation
Crotonaldehyde
Halogen
Promoter

ABSTRACT

The phase pure, unsupported intermetallic compound PtZn is intrinsically active and selective for chemoselective hydrogenation of crotonaldehyde to crotyl alcohol in the absence of any support effects or auxiliary phases. During un-promoted reaction conditions, the PtZn surface becomes platinum enriched within the XPS sampling depth with respect to the 1:1 bulk stoichiometry. Catalyst modification by co-feeding ppm levels of bromoethane results in (i) surface enrichment by zinc, (ii) pronounced formation of a chemically distinct $Zn^{\delta+}$ species and (iii) substantial improvements in selectivity toward crotyl alcohol (up to 88% at 10% reactant conversion). Bromoethane promotion acts both by suppressing formation of the undesired products and by enhancing crotyl alcohol formation, likely due to activation of the C=O bond by coordination to the $Zn^{\delta+}$ sites. Haloalkanes containing F, Cl or I do not induce any significant effects in either surface composition or electronic structure, serving only to poison the system.

1. Introduction

The chemoselective hydrogenation of α,β-unsaturated aldehydes, especially that of crotonaldehyde to crotyl alcohol, has been extensively studied due to the importance of unsaturated alcohols in a number of synthetic processes and comprehensive reviews are available [1–3]. Pt-based catalysts often involve the modification of platinum by a second metal in order to increase selectivity [4]. Common preparative methods include co-precipitation of metal precursors onto a support [5,6] or incipient wetness impregnation of a reducible metal oxide with a Pt precursor [7,8]. Depending on the procedures employed, the resulting Pt-based catalyst may contain (i) an auxiliary phase of the reducible oxide that exerts an SMSI-type effect and (ii) surface alloys or intermetallic compounds or (iii) a mixture of (i) and (ii) [9,10]. Intermetallic compounds, in contrast to alloys, are single-phase materials consisting of two or more metallic elements with an ordered crystal structure that differs from that of the constituent elements. They may be used as precursors, e.g. for Raney-type catalysts, where leaching of Al yields high surface area nickel [11,12]. Another example of their use as catalyst precursors is that of CO hydrogenation with Cu*RE* and Ni*RE* intermetallics (*RE* = rare earth) where the intermetallic compounds decompose *in situ* yielding elemental Cu or Ni supported on the corresponding rare earth oxide [13–15].

Here we are concerned with a very different application of intermetallic compounds, namely as intrinsically efficient catalysts, as opposed to catalyst precursors. An example of their effectiveness is provided by recent work on the highly selective hydrogenation of acetylene to ethene catalyzed by Pd–Ga intermetallic compounds [16–18]. It appears that such materials provide stable surface sites consisting of atomic ensembles endowed with favorable catalytic properties.

In regard to chemoselective crotonaldehyde hydrogenation, it has been reported that PtZn and PdZn alloys are formed during high temperature reduction of the Pt/ZnO and Pd/ZnO catalyst, due to the partially reducible ZnO support. This resulted in improved selectivity toward the desired product [9,19–22]. A similar effect has been reported for Pt/CeO_2 catalysts, which, after reduction at 973 K, exhibited formation of the intermetallic compound $PtCe_5$ and improved selectivity for crotyl alcohol formation [10]. In apparent contradiction to these observations, however, pure unsupported $PtCe_5$ showed no activity whatever [7]. Finally, Pt supported on α-Ga_2O_3 polymorphs delivered up to 89% selectivity to crotyl alcohol at high conversion [23], although in this case *no* intermetallic PtGa phases were detected in the post-reaction catalyst.

In order to address mechanistic issues as directly as possible, avoiding ambiguities arising from preparative methodology, possible presence of SMSI effects and the significance or otherwise of intermetallic compound formation, we studied the catalytic behavior of the well characterized, unsupported, single phase intermetal-

* Corresponding author. Fax: +44 (0) 1223/33 63 62.
E-mail address: rml1@cam.ac.uk (R.M. Lambert).

0021-9517/$ – see front matter
doi:10.1016/j.jcat.2008.11.003

lic compound PtZn. We also investigated the effects of halogen promotion on activity, selectivity, surface composition and oxidation state of the catalyst.

2. Experimental methods

2.1. Preparation of PtZn

PtZn was prepared by reaction of the appropriate stoichiometric amounts of Pt and Zn in evacuated, sealed quartz glass ampoules. 1.5174 g platinum (ChemPur 99.9%, particle size <60 μm) and 0.5088 g zinc (ChemPur 99.998%, pieces) were used to obtain 2.0262 g PtZn (7.78 mmol). The mixture of Pt and Zn was heated to 600 °C (24 °C/h), annealed at this temperature for 24 h, heated further to 900 °C (12.5 °C/h) and maintained at this temperature for 72 h. After cooling the specimen was ball milled (designated "milled sample") using a tungsten carbide crucible to yield PtZn grains of approximately 30 μm.

2.2. XRD, OES and BET

X-ray powder diffraction was performed on a Huber G670 (image plate, Cu $K\alpha_1$ with $\lambda = 1.540562$ Å). Unit-cell parameters were calculated from least square fits using the program package WinCSD [24], which utilized the BN diffraction pattern as an internal standard ($a = 2.5040$ Å, $c = 6.6612$ Å). Chemical analysis was performed by inductively coupled plasma optical emission spectrometry using a Varian Vista RL spectrometer: quoted values are the average of at least three replicates. The BET measurements were performed on a Micrometrics Gemini 2360 V5.00 using 8 point N_2 adsorption.

2.3. TEM

A Jeol 3010 electron microscope operating at 300 kV equipped with an EDX unit (Si(Li)-detector) was used for the TEM investigations. Post reaction catalyst samples consisting of PtZn dispersed in BN were loaded onto the Cu grid (holey carbon) by physical contact without the use of a solvent. The TEM images were analyzed with the DigitalMicrograph software.

2.4. XPS

High-resolution XPS data were acquired at NCESS, Daresbury, UK using a monochromatic Al $K\alpha$ source and a scan step width measurement of 0.05 eV, allowing 0.1 eV resolution. Spectra of the post-reaction catalyst samples (which consisted of PtZn physically admixed with BN powder) were taken using a low energy electron flood gun to eliminate electrostatic charging effects due to the BN. Pure Pt and pure Zn reference spectra were also acquired. Quoted binding energies are calibrated relative to the B 1*s* emission of BN taken as 190.5 eV [25]. Spectral backgrounds were fitted using the Shirley method and the Zn:Pt ratio was calculated from the integrated intensities of the Pt 4*f* and Zn 3*p* emissions, for which the photoionization cross sections are 0.227 and 0.037 Mb, respectively [26,27].

2.5. Catalytic testing

Catalytic testing was carried out at atmospheric pressure using a single pass flow microreactor with an inner diameter of 4 mm. H_2 (CP Grade BOC) was passed through a guard bed consisting of molecular sieve 4A mixed with ground Pt/ZnO in order to remove trace impurities. Liquid crotonaldehyde (99+% Aldrich), denoted CRALD, was delivered into this gas stream by a syringe pump at a rate of 0.08 ml/h where a hot zone maintained at ~120 °C vaporized the liquid *en route* to the reactor. The CRALD:H_2 molar ratio was at 1:60, corresponding to a CRALD inlet partial pressure of 17 mbar, and a weighted hourly space velocity (WHSV) of 1.73 h^{-1}. Every catalyst sample was pre-treated in hydrogen by heating to 300 °C at 5 °C/min, maintained at 300 °C for 12 h, then cooled to the reaction temperature of 200 °C (milled-reduced sample). To achieve the required gas flow characteristics, the reactor was charged with 40 mg milled PtZn powder physically mixed with 100 mg of inert boron nitride powder (Sigma Aldrich 98+%, <1 μm). When used, haloalkanes were introduced by mixing with the CRALD liquid feed to the syringe pump: the resulting haloalkane concentration was 0.545 ppm unless otherwise indicated. The haloalkanes employed were 1-fluoropentane (>99% Fluka), dichloromethane (DCM, >99.5% Sigma Aldrich), bromoethane (98+% Sigma Aldrich) and iodoethane (99% Sigma Aldrich). Analysis of the reaction products was performed by a calibrated Shimadzu 14B gas chromatograph equipped with a thermal conductivity detector and a Chromosorb Carbowax column.

3. Results and discussion

3.1. Pre-reaction catalyst characterization

Powder X-ray diffraction of the milled-reduced PtZn showed only reflections due to the single-phase material PtZn that possesses the CuAu structure (*P*4/*mmm*). The lattice parameters were determined as $a = 2.8548(4)$ Å and $c = 3.4654(7)$ Å. Chemical analysis by inductively coupled plasma optical emission spectrometry gave a composition of $Pt_{50.1(3)}Zn_{49.9(6)}$. Repeated surface area measurements of the milled-reduced PtZn catalyst gave a value of $<0.5\ m^2\,g^{-1}$, in agreement with earlier studies on similar intermetallic compounds [16]. TEM images of the milled PtZn showed crystallites of ZnO (identifiable by their characteristic lattice spacing) on the surface of the PtZn as illustrated in Fig. 1(a). Reduction at 300 °C in H_2 for 12 h resulted in the disappearance of the ZnO crystallites (Fig. 1(b)), as expected from the known behavior of ZnO [28,29].

3.1.1. XPS and TEM

Valence band XPS data were acquired of the milled and milled-reduced PtZn; reference spectra for pure Pt and pure Zn were also obtained and the results are summarized in Fig. 2. It can be seen from Fig. 2 that the valence band spectra of the two intermetallic samples differ, particularly in the Pt 5*d* 0–5 eV binding energy region. These differences are attributed to the re-incorporation of Zn into the intermetallic compound during the reduction step, in accord with the TEM results. The milled PtZn possesses a Pt-rich PtZn intermetallic surface (Table 1). This is possible because the material tolerates ~15 at% variation in composition without change of crystal structure [30]. During reduction the Zn (from the ZnO) is re-incorporated into the intermetallic compound, increasing the Zn:Pt surface ratio as the ZnO is consumed (Table 1 and Fig. 1(b)). Correspondingly, for the milled sample, the increased Zn 3*d* emission intensity at ~10.8 eV is attributable to ZnO on the surface [31,32]; this intensity is attenuated upon reduction, confirming destruction of the ZnO crystallites and re-incorporation of Zn into the intermetallic phase. Note that the reduction step stabilizes the Pt 5*d* states with respect to pure Pt (Fig. 2), a characteristic effect previously observed by Tsai et al. [33] upon alloying Pt with Zn.

The relevant Pt $4f_{7/2}$ and Zn $3p_{3/2}$ core level binding energies and calculated Zn:Pt ratios are given in Table 1. In comparison to pure Pt and pure Zn, the Pt $4f_{7/2}$ and Zn $3p_{3/2}$ binding energies in PtZn, are increased and decreased, respectively, an effect previously reported for a Pt/Zn surface alloy [34]. Note that the Zn $3p_{3/2}$

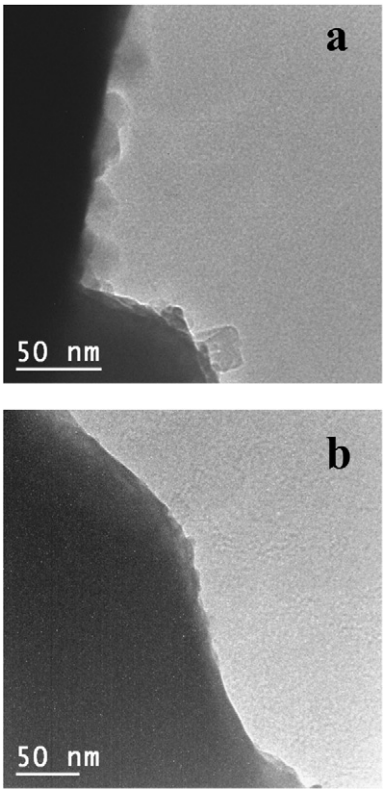

Fig. 1. (a) TEM image of milled PtZn particles with ZnO crystallites on the surface; (b) a milled-reduced PtZn particle.

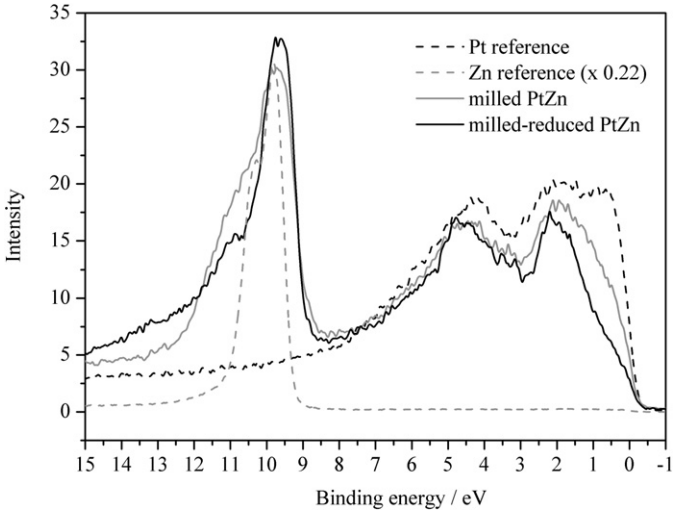

Fig. 2. XP spectra of the PtZn valence band region. Pure Pt and pure Zn spectra are shown for reference.

Table 1
Core level binding energies of Pt $4f_{7/2}$ and Zn $3p_{3/2}$ for PtZn as well as Pt and Zn as references.

Sample	Pt $4f_{7/2}$ (FWHM) (eV)	Zn $3p_{3/2}$ (FWHM) (eV)	Zn:Pt ratio
Milled PtZn	71.2 (0.7)	88.3 (2.6)	0.91
Milled-reduced PtZn	71.2 (0.7)	88.2 (2.6)	1.19
Pt reference	71.1 (0.8)	–	–
Zn reference	–	88.6 (2)	–

emission cannot be used to discriminate between ZnO and Zn [35–39] in part due to wide range of reported values for the spin orbit splitting of the Zn $3p_{3/2}$ and Zn $3p_{1/2}$ final state.

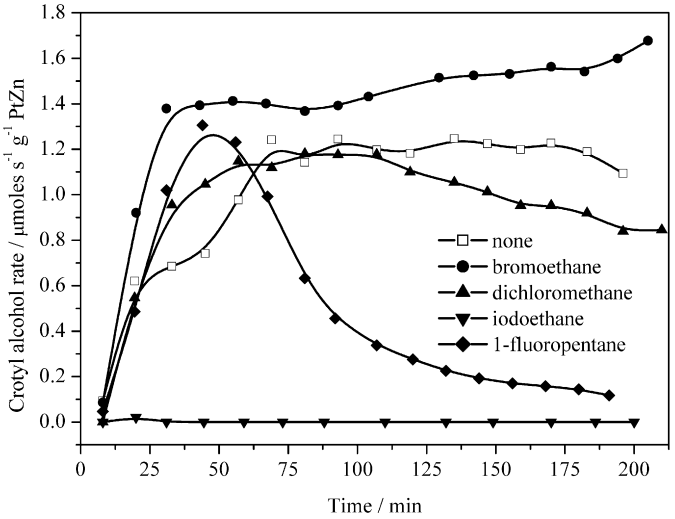

Fig. 3. Time dependence of rate of hydrogenation of crotonaldehyde to crotyl alcohol in the presence of 0.545 ppm haloalkanes.

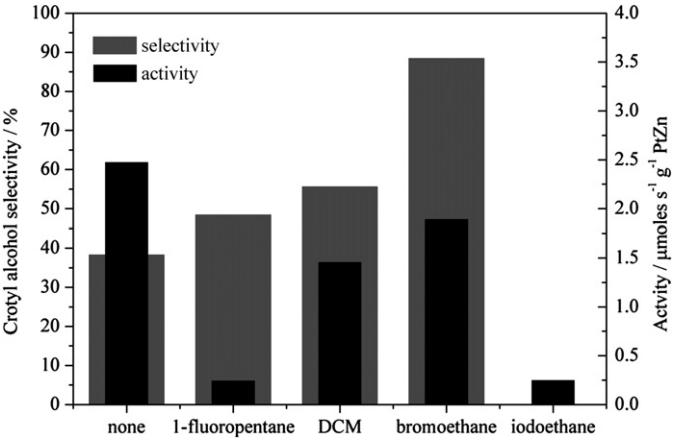

Fig. 4. Crotyl alcohol selectivity and overall rate of conversion at 200 min (quasi-steady-state) in the presence of 0.545 ppm haloalkanes.

In summary, the XRD, OES, TEM and XPS results show that the freshly milled catalyst consists of ZnO nanocrystals decorating a Pt-rich bimetallic surface, Zn:Pt = 0.91. The ZnO is readily reduced by hydrogen to elemental Zn which is re-incorporated into the intermetallic phase, and, within the XPS sampling depth, the surface composition of this material is Zn:Pt = 1.19.

3.1.2. Catalytic testing

The time dependence of the resulting rates of crotyl alcohol formation for un-promoted and haloalkane-modified catalysts are presented in Fig. 3 and the corresponding steady state selectivities and activities at a reaction time of 200 min are shown in Fig. 4. Formation of the undesired products, butyraldehyde (Fig. 5) and butanol were poisoned by all the haloalkanes, whereas bromoethane alone strongly promoted selectivity toward crotyl alcohol formation (up to 88%) accompanied by a relatively modest loss of activity. Dichloromethane was significantly less effective than bromoethane, leading to a small increase in selectivity with a large decrease in activity. Fluoropentane strongly poisoned activity, leaving selectivity almost unchanged, and poisoning by iodoethane drastically reduced catalyst selectivity, a fact that is understandable in the light of the XPS findings presented below.

The absence of elemental Pt (e.g. formed by segregation) in the pre-reaction XRD patterns of the milled and milled-reduced samples is consistent with the observations in the reactor study, as

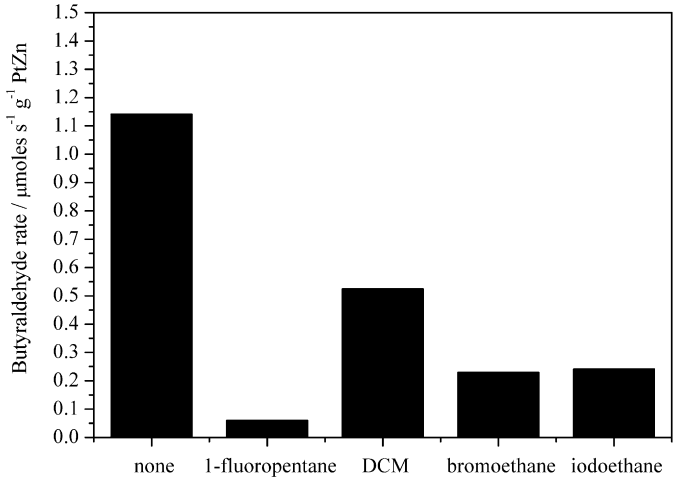

Fig. 5. Rate of formation of butyraldehyde at 200 min (quasi-steady-state) in the presence of 0.545 ppm haloalkanes.

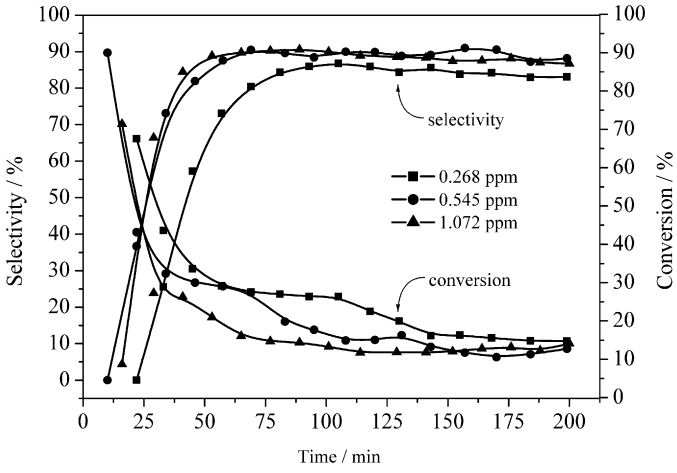

Fig. 6. Crotyl alcohol selectivity and overall rate of conversion *versus* time on line for 3 different bromoethane concentrations.

monometallic Pt species are known to show significant activity and selectivity to the undesired butyraldehyde and butanol already at significantly lower reaction temperatures [1–3].

Fig. 6 shows the time dependence of crotyl alcohol selectivity and reactant conversion for a range of bromoethane concentrations. The decreases in conversion observed at ~35, ~75 and ~110 min for 1.072, 0.545 and 0.268 ppm bromoethane, are due to reduction in the rate of butanol formation. These correspond with smaller increases in the rates of crotyl alcohol (Fig. 3) and butyraldehyde formation, resulting in the selectivity to crotyl alcohol remaining almost unchanged at ~85%, with a ~10% reduction in reactant conversion. These data show that the steady state condition of the catalyst surface is essentially independent of the bromoethane concentration, which affects only the time at which the steady state is attained. Moreover, once the steady state was reached (~200 min) *switching off the bromoethane feed had little effect on the selectivity* which remained at ~85%. This is consistent with limited uptake of Br on the catalyst surface, where it exerts a beneficial effect for reasons explained below. In the present case, analysis of the reactor exit gas showed the presence of ethene, consistent with bromine deposition according to $C_2H_5Br \rightarrow C_2H_4(g) + Br(a) + H(a)$. Such dehalogenation reactions of haloalkanes by metals surfaces are well known [40–42]. In passing we note that the minor response of the system to DCM is unlikely to be due to the inability of this molecule to deposit Cl on the catalyst surface. From studies carried out on both single crystals under UHV conditions and with dispersed metal catalysts, it is known that hydrodechlorination of DCM with deposition of adsorbed Cl is facile on Pt, Pd and Ir surfaces, occurring even at room temperature [43–45]. Therefore it is plausible to suppose that DCM acts in a similar way in the present case.

Table 2
Lattice parameters of post reaction PtZn catalysts.

Catalyst	PtZn lattice parameter (Å)	
	a	*c*
No haloalkane	2.8552(3)	3.4672(4)
1-Fluoropentane	2.8563(3)	3.4690(8)
Dichloromethane	2.8546(8)	3.466(1)
Bromoethane	2.8543(6)	3.4669(9)
Iodoethane	2.8549(6)	3.466(1)

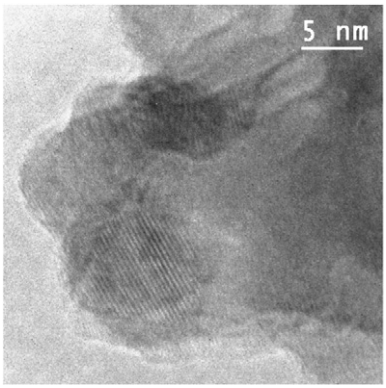

Fig. 7. TEM image from post reaction catalyst after promotion by bromoethane. Lattice fringes of PtZn (001) are clearly visible while no ZnO is observed.

3.2. Post-reaction catalyst characterization

3.2.1. XRD

Table 2 lists the lattice parameters of the post reaction catalysts using BN as internal standard. PtZn was the only detectable phase. No significant changes were observed between the post reaction catalyst lattice parameters, we therefore conclude that the effect of haloalkanes on catalyst performance is not connected with bulk transformations and must be a surface-related phenomenon.

3.2.2. TEM and XPS

Fig. 7 presents a TEM picture of a bromoethane-modified PtZn particle. There were no observable differences in the TEM between any of the post reaction catalysts or the milled-reduced pre-reaction catalyst. No ZnO crystallites were detected, confirming that the only bulk active-phase present in the catalyst was the intermetallic compound PtZn.

With 1486.6 eV Al Kα radiation, the XPS sampling depth was approximately 1.5 nm [46]. Zn:Pt atomic ratios were calculated based on the relevant photoionization cross sections and are presented in Table 3 with representative spectra shown in Fig. 8. The only halogen emission observed in the post-reaction catalysts samples was that of I 3*d*, the others being at or below the detection limit. Quantification of the I 3*d* intensity indicates that the iodine coverage corresponded to approximately an I:Pt surface atomic ratio of ~1, which is consistent with the drastic deactivation caused by iodoethane. Control experiments showed that halogen deposition did not occur on the BN diluent.

The catalyst exposed to bromoethane exhibited two important differences from the others in regard to the Pt and Zn spectra. First, the Zn:Pt ratio was 1.82, significantly larger than that char-

Table 3
Peak parameters and resulting Pt:Zn ratios of the fitted XPS core level spectra of the different PtZn catalysts.

Peak	Haloalkane	Binding energy[a] (eV)	FWHM (eV)	Zn:Pt ratio
Pt $4f_{7/2}$	none	71.2	0.8	0.61
Zn $3p_{3/2}$	none	88.2	2.6	
Pt $4f_{7/2}$	1-fluoropentane	71.2	0.8	0.85
Zn $3p_{3/2}$	1-fluoropentane	88.1	2.6	
Pt $4f_{7/2}$	DCM	71.3	0.9	0.76
Zn $3p_{3/2}$	DCM	88.4	2.6	
Pt $4f_{7/2}$	bromoethane	71.3	1.0	1.82
Zn $3p_{3/2}$	bromoethane	88.2	2.6	
$Zn^{\delta+}$ $3p_{3/2}$	bromoethane	89.7	2.6	
Pt $4f_{7/2}$	iodoethane	71.3	0.8	0.78
Zn $3p_{3/2}$	iodoethane	88.2	2.6	

[a] For Pt $4f_{7/2}$ and Zn $3p_{3/2}$ photoelectrons with a SOS of 3.33 and 2.73 eV, respectively.

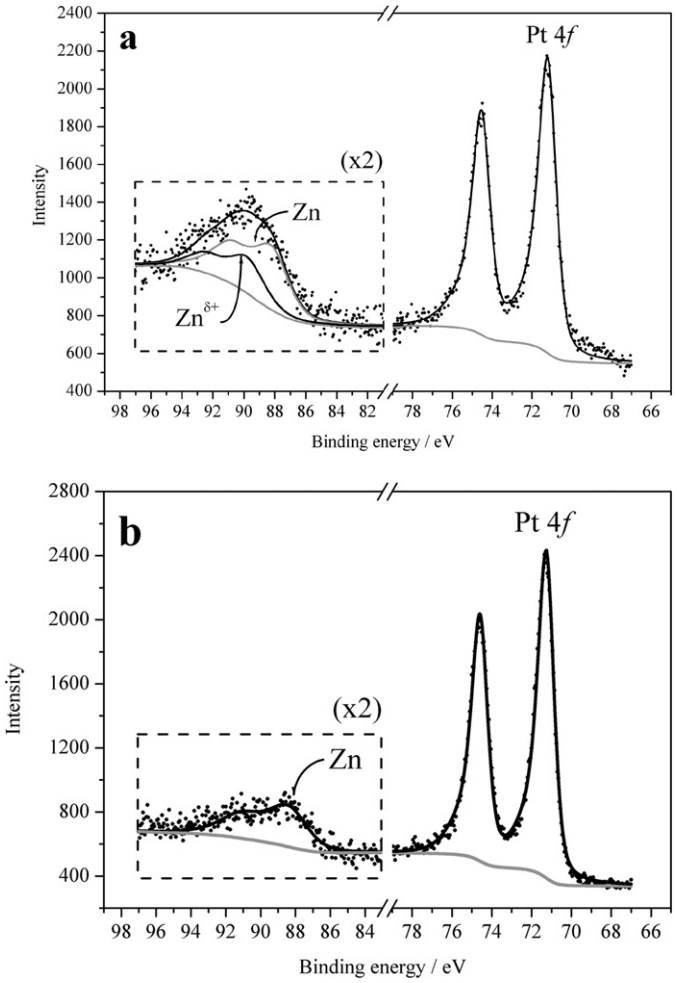

Fig. 8. Core level XP spectra of post reaction catalysts promoted by (a) bromoethane and (b) dichloromethane. Note the additional $Zn^{\delta+}$ component in the bromoethane treated catalyst and an increase in the integrated signal of Zn $3p$ with respect to Pt $4f$ compared to (b).

acteristic of the pre-reaction catalyst (1.19), whereas for all other haloalkane-treated catalysts this ratio was much less than 1. Second, bromoethane induced the formation of an additional chemically distinct Zn species (denoted $Zn^{\delta+}$) with a much higher binding energy (by ~1.5 eV) than that characteristic of Zn in the intermetallic compound. The ratio of $Zn^{\delta+}$:Zn intensities was 0.49, therefore $Zn^{\delta+}$ constituted an atomic fraction of 0.2 of the total surface composition. The Br $3d$ emission lies close to the strong Pt $4f$ emission. Close inspection of the 68–69 eV region in Fig. 8(a) reveals a slight deviation from the fitted intensity. *If* this is due to Br $3d$, then we may deduce a ratio of $Zn^{\delta+}$:Br > 4.

The best-known example of strong halogen-promoted selectivity enhancement of a catalytic reaction is that of the Ag-catalyzed epoxidation of ethene. Chloroalkanes are continuously fed to the process gas at ppm levels to maintain the surface coverage of chlorine atoms at the optimum level, thereby maximizing epoxidation selectivity [47]. In this study it is proposed that the haloalkane deposit halogen atoms permanently on the catalyst surface.

4. Conclusions

1. Although some decomposition of the unsupported intermetallic compound PtZn occurs during milling in the presence of oxygen, yielding crystals of ZnO that decorate the PtZn grains, under hydrogenation conditions the solid phase consists of pure PtZn, with some surface enrichment by Pt. The observed chemoselective activity toward crotyl alcohol formation is therefore an intrinsic property of the well-defined intermetallic compound PtZn, independent of any effects due to a solid support.

2. Of all the halogens, bromine was uniquely effective in strongly promoting crotyl alcohol selectivity from 37% to 88%, accompanied by some loss of activity, when 0.545 ppm of bromoethane was added to the reaction gas. In part, bromine promotion acts by suppressing formation of the undesired products, possibly by deactivating sites that would otherwise adsorb the reactant in a mode that favored C=C hydrogenation. Dichloromethane had relatively little effect on catalyst performance whereas iodoethane and 1-fluoropentane acted as strong poisons.

3. XPS data for the post-reaction catalyst demonstrate that bromoethane induces strong enrichment of the catalyst surface by zinc and substantial formation of a chemically distinct $Zn^{\delta+}$ species. It therefore seems likely that this Br-induced species acts to activate the C=O bond by coordination to $Zn^{\delta+}$ sites, thus favoring formation of the unsaturated alcohol.

The decrease in total activity of the catalysts exposed to haloalkanes is attributed to a site blocking mechanism. Bromoethane is the only halogenated hydrocarbon to increase the rate of crotyl alcohol formation while reducing the rate of butyraldehyde and butanol formation.

Acknowledgments

E.G. acknowledges financial support from the UK Engineering and Physical Sciences Research Council. M.A. thanks the Alexander von Humboldt foundation for the award of a Feodor Lynen Fellowship and the European Commission for the award of a Marie Curie Fellowship.

Supplementary material

The online version of this article contains additional supplementary material.

Please visit DOI: 10.1016/j.jcat.2008.11.003.

References

[1] V. Ponec, Appl. Catal. A 149 (1997) 27.
[2] P. Maeki-Arvela, J. Salmi, T. Murzin, D. Yu, Appl. Catal. A 292 (2005) 1.
[3] F.F. Bernard Coq, Coord. Chem. Rev. 178–180 (1998) 1753.
[4] T.B.L.W.N. Marinelli, V. Ponec, J. Catal. 151 (1995) 431.
[5] J. Silvestre-Albero, F. Coloma, A. Sepulveda-Escribano, F. Rodriguez-Reinoso, Appl. Catal. A 304 (2006) 159.
[6] J. Silvestre-Albero, F. Rodriguez-Reinoso, J.A. Anderson, J. Catal. 223 (2004) 179.
[7] M. Abid, V. Paul-Boncour, R. Touroude, Appl. Catal. A 297 (2006) 48.
[8] K.T. Liberkova, R. Touroude, J. Mol. Catal. A 180 (2002) 221.
[9] M.J. Consonni, D.Y. Murzin, R. Touroude, J. Catal. 188 (1999) 165.
[10] M. Abid, G. Ehret, R. Touroude, Appl. Catal. A 217 (2001) 219.

[11] M. Raney, US 1628190 (1927).
[12] M. Raney, US 1563587 (1925).
[13] R.M. Nix, T. Rayment, R.M. Lambert, J.R. Jennings, G. Owen, J. Catal. 106 (1987) 216.
[14] C.M. Hay, R.M. Lambert, R.M. Nix, G. Owen, T. Rayment, Appl. Catal. 37 (1988) 291.
[15] V.T. Coon, W.E. Wallace, R.S. Craig, G.J. McCarthy, J.J. Rhyne, Rare Earths in Modern Science and Technology, Plenum Press, New York, 1978, p. 93.
[16] K. Kovnir, J. Osswald, M. Armbrüster, R. Giedigkeit, T. Ressler, Yu. Grin, R. Schlögl, Stud. Surf. Sci. Catal. 162 (2006) 481.
[17] K. Kovnir, M. Armbrüster, D. Teschner, T. Venkov, F.C. Jentoft, A. Knop-Gericke, Yu. Grin, R. Schlögl, Sci. Technol. Adv. Mater. 8 (2007) 420.
[18] (a) J. Osswald, R. Giedigkeit, R.E. Jentoft, M. Armbrüster, F. Girgsdies, K. Kovnir, T. Ressler, Yu. Grin, R. Schlögl, J. Catal. 258 (2008) 210;
(b) J. Osswald, K. Kovnir, M. Armbrüster, R. Giedigkeit, R.E. Jentoft, U. Wild, Yu. Grin, R. Schlögl, J. Catal. 258 (2008) 219.
[19] F. Ammari, J. Lamotte, R. Touroude, J. Catal. 221 (2004) 32.
[20] N. Iwasa, S. Masuda, N. Ogawa, N. Takezawa, Appl. Catal. A 125 (1995) 145.
[21] N. Iwasa, S. Masuda, N. Ogawa, N. Takezawa, Bull. Chem. Soc. Jpn. 71 (1998) 1451.
[22] A. Karim, T. Connant, A. Datye, J. Catal. 243 (2006) 420.
[23] E. Gebauer-Henke, J. Grams, E. Szubiakiewicz, J. Farbotko, R. Touroude, J. Rynkowski, J. Catal. 250 (2007) 195.
[24] L.G. Akselrud, P.Yu. Zavalii, Yu. Grin, V.K. Pecharsky, B. Baumgartner, E. Wölfel, Mater. Sci. Forum 133–136 (1993) 335.
[25] T. Goto, T. Hirai, J. Mater. Sci. 7 (1988) 548.
[26] J.J. Yeh, I. Lindau, At. Data Nucl. Data Tables 32 (1985) 1.
[27] C.D. Wagner, W.M. Riggs, L.E. Davis, J.F. Moulder, G.E. Muilenberg, in: J. Chastain, R.C. King (Eds.), Handbook of XPS, Physical Electronics Inc., Eden Prairie, MN, 1979.
[28] L. Wang, G.W. Qiao, H.Q. Ye, K.H. Kuo, Y.X. Chen, J. Electron Microsc. Technol. 10 (1988) 7.
[29] F. Boccuzzi, A. Chiorino, G. Ghiotti, F. Pinna, G. Strukul, R. Tessarit, J. Catal. 126 (1990) 381.
[30] Z. Moser, in: T.B. Massalski (Ed.), Binary Alloy Phase Diagrams, second ed., ASM International, Materials Park, 1990, p. 3153.
[31] S.W. Gaarenstroom, N. Winograd, J. Chem. Phys. 67 (1977) 3500.
[32] D.W. Langer, C.J. Vesely, Phys. Rev. B 2 (1970) 4885.
[33] A.P. Tsai, S. Kameoka, Y. Ishii, J. Phys. Soc. Jpn. 73 (2004) 3270.
[34] J.A. Rodriguez, M. Kuhn, J. Chem. Phys. 102 (1995) 4279.
[35] G. Schön, J. Electron Spectrosc. Relat. Phenom. 2 (1973) 75.
[36] B.R. Strohmeier, D.M. Hercules, J. Catal. 86 (1984) 266.
[37] J.M. Mariot, G. Dufour, Chem. Phys. Lett. 50 (1977) 219.
[38] L. Ley, S.P. Kowalczyk, F.R. McFeely, R.A. Pollak, D.A. Shirley, Phys. Rev. B 8 (1973) 2392.
[39] C.J. Vesely, D.W. Langer, Phys. Rev. B 4 (1971) 451.
[40] Y.H. Choi, W.Y. Lee, J. Mol. Catal. A 174 (2008) 193.
[41] M.F. Kadodwala, A.A. Davis, G. Scragg, B.C.C. Cowie, M. Kerbarb, D.P. Woodruff, R.G. Jones, Surf. Sci. 392 (1997) 199.
[42] S. Haq, S.C. Laroze, C. Mitchell, N. Winterton, R. Rava, Surf. Sci. 531 (2003) 145.
[43] Y.-N. Wang, J.A. Marcos, G.W. Simmons, K. Klier, J. Phys. Chem. 94 (1990) 7597.
[44] V. Dal Santo, C. Dossi, S. Recchia, P.E. Colavita, G. Vlaic, R. Psaro, J. Mol. Catal. A 182–183 (2002) 157.
[45] C.T. Reeves, R.J. Meyer, C.B. Mullins, J. Mol. Catal. A 202 (2003) 135.
[46] S. Tanuma, C.J. Powell, D.R. Penn, Surf. Interface Anal. 21 (1993) 165.
[47] R.M. Lambert, R.L. Cropley, A. Husain, M.S. Tikhov, Chem. Commun. 10 (2003) 1184.